

Weighted and well-balanced anisotropic diffusion scheme for image denoising and restoration

V. B. Surya Prasath*

Department of Computer Science, University of Missouri-Columbia, MO 65211-2060, USA

D. Vorotnikov

CMUC, Department of Mathematics, University of Coimbra, 3001-454 Coimbra, Portugal

Abstract

Anisotropic diffusion is a key concept in digital image denoising and restoration. To improve the anisotropic diffusion based schemes and to avoid the well-known drawbacks such as edge blurring and ‘staircasing’ artifacts, in this paper, we consider a class of weighted anisotropic diffusion partial differential equations (PDEs). By considering an adaptive parameter within the usual divergence process, we retain the powerful denoising capability of anisotropic diffusion PDE without any oscillating artifacts. Well-balanced flow version of the proposed scheme is considered which adds an adaptive fidelity term to the usual diffusion term. The scheme is general, in the sense that, different diffusion coefficient functions can be utilized according to the need and imaging modality. To illustrate the advantage of the proposed methodology, we provide some examples, which are applied in restoring noisy synthetic and real digital images. A comparison study with other anisotropic diffusion based schemes highlight the superiority of the proposed scheme.

Key words: Image restoration, Edge preserving, Nonlinear diffusion, Biased anisotropic diffusion, Well-balanced flow

*Corresponding author. Tel.: +1 573-882-8391 Fax: +1 573-882-8318.
Email addresses: prasaths@missouri.edu (V. B. Surya Prasath), mitvorot@mat.uc.pt (D. Vorotnikov)

1. Introduction

Image denoising is one of the foremost tasks in digital image processing pipeline. There exist various methodologies for removing noise in images and the areas of image restoration and edge detection have been considered by many authors. Starting with the pioneering work of Perona and Malik [1], diffusion based partial differential equations (PDEs) are widely used in image noise removal and edge detection, see [2] for a review. Let u_0 be the noisy image which needs to be restored by removing noise without removing salient structures in it. Mathematically, $u_0 : \Omega \rightarrow \mathbb{R}$ represents a noisy version of a true image, and it is obtained by the following imaging process

$$u_0 = u + n, \quad (1)$$

here we assume that the noise process n is additive Gaussian noise with known mean and variance σ_n . The image domain $\Omega \subset \mathbb{R}^2$ is a bounded domain, usually a rectangle.

The Perona-Malik scheme (PM) can be written as a time dependent PDE, for $x \in \Omega$

$$\frac{\partial u(x, t)}{\partial t} = \operatorname{div} (c(|\nabla u(x, t)|) \nabla u(x, t)) \quad (2)$$

with $u(x, 0) = u_0(x)$, i.e. the input noisy image is the initial datum, and the above PDE is run for a finite time $T > 0$ to obtain the denoised image $u(\cdot, T)$. The choice of the diffusion function $c : [0, \infty) \rightarrow [0, \infty)$ is important in controlling the smoothing and even enhancement of edges. In [1] the following two diffusion functions are considered

$$c_{pm1}(s) = \frac{1}{1 + (s/K)^2}, \quad c_{pm2}(s) = \exp(-(s/K)^2) \quad (3)$$

where $K > 0$ is the contrast parameter. By such choices of nonlinear functions, PM PDE (2) avoids the over-smoothing property of the heat equation. Good numerical results coupled with the fact that, theoretically, the PM PDE with diffusion functions (3) is ill-posed [3], generated an enormous interest in the

25 mathematical image processing community, see [2] for a review. Moreover, an
26 anisotropic PDE such as (2) can be considered as a gradient descent of a suitable
27 energy functional [4, 5, 6]. The success of the anisotropic diffusion can be
28 attributed to the fact that the PDE can be effectively discretized [7].

29 Though the PDE based schemes exhibit good denoising behavior, sometimes
30 they can give artifacts such as staircasing or blocky regions. These drawbacks
31 can occur due to various reasons, the primary one is the use of gradients to
32 control diffusion. To avoid this, there have been efforts to use better control
33 mechanisms for inhibiting diffusion in flat regions of the image. These tech-
34 niques can be classified into three broad categories: (1) Use spatial or time
35 regularization of the gradients [8, 9, 10, 11] (2) Use a separate PDE to get
36 better diffusion coefficients [12, 13, 14, 15] (3) spatially adaptive diffusion co-
37 efficients [16, 17, 18, 19, 20, 21, 22]. Though the spatial regularization reduces
38 the effect of noise in gradient computations, it can still give staircasing effects
39 and can have poor localization of edges. In coupled PDE based schemes, apart
40 from the expense of solving another PDE to get the edge map, it can inherit the
41 problems of the original diffusion PDE. Spatially adaptive diffusion coefficient
42 based scheme tries to balance these issues by providing a robust edge map for
43 the diffusion to act upon. Recently, nonlocal diffusion operators were considered
44 in [23, 24, 25] with corresponding wellposedness results. Another approach is
45 to use higher order diffusion models [26].

46 Here we consider an adaptive scheme which is based on this methodology.
47 Recently, Barcelos et al [27, 28] considered a well-balanced model inspired by the
48 idea of mean curvature motion [29] and Nordstörn’s biased PDE [30] approach.
49 In this paper, we generalize such a model and consider weighted anisotropic
50 diffusion schemes which incorporates adaptive information computed from the
51 image at scale t . Moreover, following Smolka [31] a modification of the im-
52 age fidelity term is also done to improve the denoising capability of the PDE.
53 Following [27], wellposedness of the proposed scheme is proved using the the-
54 ory of viscosity solutions. Numerical examples in image denoising are given to
55 highlight the proposed model.

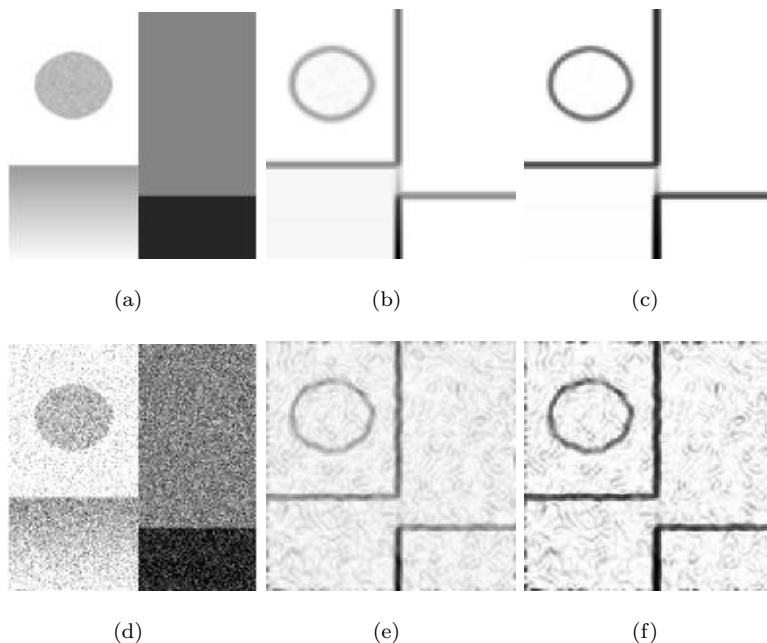


Figure 1: Diffusion PDE denoising depends on good edge maps and if the noise persists through the iterations, it leads to staircasing artifacts in the denoised version. (a) Original *Kikis* image used in the experiments (b) Smoothed gradient $|G_\sigma \star \nabla u|$ of the original image, $\sigma = 2$ (Black signifies higher values and white lower) (c) Edge map of the original image computed using the diffusion function c_{pm1} from (3) with $K = 20$ (d) Noisy image obtained by adding Gaussian noise of $\sigma_n = 30$ to the original image (e) Smoothed gradient $|G_\sigma \star \nabla u_0|$ of the noisy image, $\sigma = 2$ (f) Edge map of the noisy image computed using the diffusion function c_{pm1} from (3) with $K = 20$.

56 The rest of the paper is organized as follows. Section 2.1 introduces the
57 proposed weighted anisotropic diffusion scheme and a modification based on
58 the well-balanced flow model of [27] is presented. Section 4 details the numer-
59 ical aspects and shows comparison denoising results on noisy images. Finally,
60 Section 5 concludes the paper.

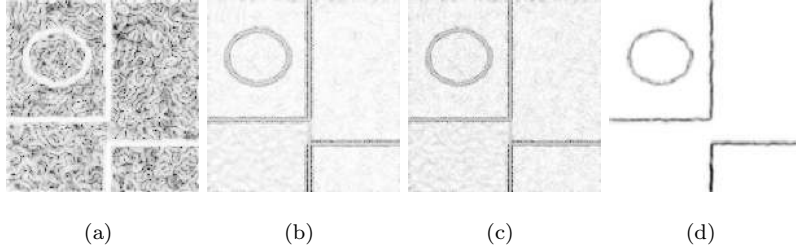


Figure 2: Edge stopping Vs adaptive diffusion coefficients: (a) Edge stopping function of the noisy image $(1 + |G_\sigma \star \nabla u_0|^2)^{-1}$ (b) Inverse gradient based $c(x, |\nabla u|) = \alpha(x) |\nabla u|$, where $\alpha(x) = 1/(1 + K |G_\sigma \star \nabla u_0|^2)$ (c) Slowed diffusion $c(x, |\nabla u|) = (G_\sigma \star \nabla u) / (1 + |G_\sigma \star \nabla u|^2 / K^2)$ (d) Canny edge detector based $c(x, |\nabla u|) = \alpha(x) |\nabla u|$, where $\alpha(x) = 1 - G_\sigma \star \text{Canny}(u(x, t))$.

61 2. Weighted well-balanced anisotropic diffusion

62 2.1. Well-balanced flow equation

63 The well-balanced flow (WBF) equation studied by Barcelos et al. [27, 28] is
 64 based on total variation and can be generalized to the divergence process such
 65 as the Perona-Malik diffusivity:

$$\frac{\partial u}{\partial t} = g |\nabla u| \operatorname{div} (c(|\nabla u|) \nabla u) - \lambda(1 - g)(u - u_0) \quad (4)$$

66 where $g(u \star \nabla G_\sigma) = (1 + |G_\sigma \star \nabla u|^2)^{-1}$ is known as the edge stopping function.
 67 The pre-smoothing with $G_\sigma(x) = (2\pi\sigma)^{-1} \exp(-|x|^2 / 2\sigma)$, a Gaussian kernel of
 68 width σ , is used to avoid noisy oscillations from the gradient computations. If
 69 the diffusion function is $c(s) = s^{-1}$ (total variation (TV) [32]) then we recover
 70 the model studied in [27]. This TV diffusion function, in a sense, represents
 71 the borderline case from a class of decreasing diffusion functions. More faster
 72 decreasing functions can also be used, for example [33], $c(s) = s^{-2}$, though
 73 wellposedness results for (4) can not be obtained in these cases.

74 2.2. Weighted anisotropic diffusion

75 Figure 1 shows the synthetic image used in our experiments. It consists
 76 of homogeneous regions separated by strong edges, gradual slope and a circle
 77 object with noisy oscillations. Figures 1(b) & (c) show the smoothed gradient

78 and diffusion function c_{pm1} computed using the original image. These images
79 show that the edge map of the image is captured by the diffusion coefficient
80 and highlights its importance in restoration. The diffusion coefficient c used
81 in the PDE (4) can be influenced greatly by noise and gradient computations
82 can be oscillatory. Figures 1(e)&(f) show the smoothed gradient and diffu-
83 sion function c_{pm1} values, respectively, computed using the noisy image $|\nabla u_0|$.
84 Clearly, an edge map obtained in this way can lead to diffusion leakage and fur-
85 ther iterations can propagate these oscillations which gives staircasing artifacts.
86 Moreover, these gradient based diffusion functions give rise to edge pruning un-
87 der evolution [34]. Hence, we need to use an adaptive measure which can give
88 a pixel-wise information to the diffusion function $c(x, |\nabla u|)$ in the divergence
89 process. We propose the following class of functions for the diffusion PDE (6):

$$c(x, |\nabla u|) = \alpha(x) c_g(|\nabla u|) \quad (5)$$

90 Here, α is the adaptive parameter estimated at each pixel $x \in \Omega$. The function
91 c_g depends on the gradient image $|\nabla u|$ and can be chosen similar to (3). Note
92 that, similar adaptive diffusion function studied in [16] is done for TV gradient
93 function, i.e $c_g(|\nabla u|) = |\nabla u|$. Further, the proposed scheme (6) is modified to
94 include the balance term of [27], and thus provides a well-balanced flow in terms
95 of noise removal and edge preservation. Thus, we consider the following general
96 model (Nordström’s biased version [30]) based on PM PDE from Eqn. (2):

$$\frac{\partial u}{\partial t} = g \operatorname{div} (c(x, |\nabla u|) \nabla u) - \lambda(1 - g)(u - u_0) \quad (6)$$

97 where the parameter λ balances the fidelity term and the usual divergence pro-
98 cess. Here, we made the diffusion function $c(x, |\nabla u|)$ to depend on the spatial
99 variable $x \in \Omega$ as well as the magnitude of the gradient $|\nabla u|$, which implies the
100 introduction of inhomogeneity into the PDE. For this reason we call the PDE
101 in Eqn (6) as weighted and well-balanced flow (WWBF) equation.

102 2.3. Choice of diffusion function, weight and other issues

103 The original Perona-Malik diffusion functions (3) represent two different be-
104 haviors with respect to the way the diffusion propagation is carried out. The

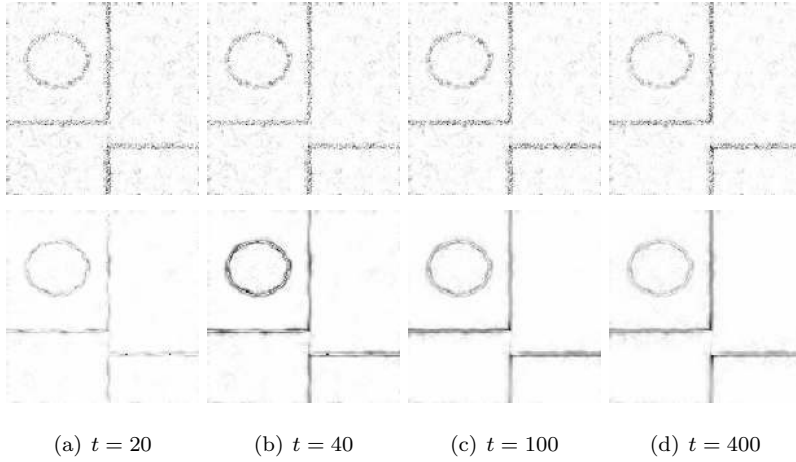


Figure 3: Effect of the balancing (fidelity term) on denoising the *Kikis* noisy image ($\sigma_n = 30$) using the PM PDE (2) with c_{pm1} . Each image shows the fidelity at different time stamps $t = 20, 40, 100, 200$ (Black signifies higher values and white lower). Top row: classical fidelity $(1 - g) |u(x, t) - u_0(x)|$ Bottom row: adaptive fidelity $(1 - g) |u(x, t) - u(x, t - 1)|$.

105 c_{pm1} prefers flat regions over edges and can inhibit higher gradients faster than
 106 the c_{pm2} function. To make the presentation simple, throughout the arti-
 107 cle we use the c_{pm1} diffusion function in all the PDEs. There exists various
 108 choices [17, 19, 21, 22] for the weight function α in Eqn. (6). The first choice is
 109 to use the classical inverse gradient approach [17], $\alpha(x) = (1 + K |\nabla u_0(x)|^2)^{-1}$,
 110 the other two choices are the slowed diffusion approach [35], and the Canny
 111 edge detector based parameter [22], $\alpha(x) = 1 - G_\sigma \star Canny(u(x, t))$. Figure 2
 112 illustrate the usage of adaptive diffusion coefficient against the traditional edge
 113 stopping function in front of the divergence term. Note that the edge stopping
 114 function g acts as the ‘rate’ of the diffusion whereas the adaptive coefficient α
 115 controls the ‘amount’ of diffusion. In this sense, both the edge stopping function
 116 g and the adaptive parameter α give complementary information for solving the
 117 denoising problem. Table 1 provides a succinct comparison of different weight
 118 functions from the literature with respect to image restoration. We utilize the
 119 inverse gradient function as the weight in the numerical experiments reported
 120 here and observed similar results with other adaptive parameter based functions.

Table 1: Comparison of different weight functions for image denoising and restoration. Note that G_σ is a Gaussian kernel, $\mathbf{1}_A$ is the indicator function for a set A , χ_c is a smooth edge indicator function, $Var_{\mathcal{N}_x}^2(u)$ is the local variance of the image function u , for more details we refer to the corresponding references.

Ref.	$\alpha(x)$	Advantages	Disadvantages
[21]	$(1 + G_\sigma \star \nabla u_0(x) ^2)^{-1}$	No staircasing artifacts	Small-scale edges lost
[35]	$\mathbf{1}_{(0.5,1]}(G_\sigma \star \nabla u(x,t))/(1 + G_\sigma \star \nabla u ^2/K^2)$	No diffusion at edges	Noise remain along edges
[19]	$1 + M_c \chi_c$, $M_c \gg 0$ constant	Edge indication	Excessive blurring
[22]	$1 - G_\sigma \star Canny(u(x,t))$	Retains multi-scale edges	Cannot handle high noise
[36]	$\exp(-\Theta(Var_{\mathcal{N}_x}^2(u(x,t)), \theta)/\delta)$	Contextual discontinuities	Stippled pattern artifacts
[37]	$\mathbf{1}_I + \mathbf{1}_{I^c} \exp(-(G_\sigma \star \nabla u(x) /K)^2)$	Handles impulse noise	Cannot handle textures

121 Note that the fidelity term in Eqn. (6) provides a complementary informa-
122 tion using the noisy image $u(x,0) = u_0(x)$. To further increase the denoising
123 capability, we can make the classical image fidelity term $(u(x,t) - u(x,0))$ in
124 Eqn. (6) to be adaptive, i.e., $(u(x,t) - u(x,t-1))$, see Smolka [31]. Figure 3
125 shows the effect of fidelity on denoising the noisy *Kikis* image (Figure 1(d))
126 using the PM PDE (2) with diffusion coefficient c_{pm1} . Comparing the adap-
127 tive approach (Figure 3, bottom row) with the classical fidelity (Figure 3, top
128 row), we can see that the adaptive process keeps edge details as the iteration
129 increases. This, in turn, will aid the proposed WWBF PDE (6) to smooth the
130 noisy image without destroying the salient edges.

131 **Remark 1.** *The balancing term parameter λ can also be made adaptive, see*
132 *Gilboa et al [38]. A spatially adaptive balance parameter $\lambda(x)$ can keep the*
133 *textural component in the restored image u , while keeping the fidelity constraint.*

134 **Remark 2.** *Further generalizations of the well-balanced flow are also possible.*
135 *For example, the diffusion coefficient can also be made to depend on the image*
136 *u , i.e., $c(x,u,|\nabla u|)$. Such a generalization can lead to different diffusion flows*
137 *and can be designed to influence the restoration process.*

138 The wellposedness of the proposed PDE (6) can be proved using the vis-

139 viscosity solution theory and its discretized version satisfies the usual scale-space
 140 properties as well.

141 3. Theoretical considerations

142 3.1. Preliminaries

143 Following [27, 39], we study the proposed PDE

$$\frac{\partial u}{\partial t} = g(G * \nabla u) \operatorname{div} (c(x, |\nabla u|) \nabla u) - \lambda(1 - g(G * \nabla u))(u - u_0) \quad (7)$$

144 using the viscosity solution theory of P. L. Lions et al [40]. Here we admit
 145 generic convolution kernels G , which, in particular, can be the Gaussian kernels
 146 G_σ , and arbitrary spatial dimension $n > 1$.

147 Throughout this section, we employ Einstein's summation convention. Let
 148 us first introduce two auxiliary functions depending on x and p from \mathbb{R}^n , a
 149 symmetric-matrix-valued one a and a vector one χ . We denote

$$a_{ij}(x, p) = c(x, |p|) \delta_{ij} + c_y(x, |p|) \frac{p_i p_j}{|p|}, \quad (8)$$

150

$$\chi_i(x, p) = \frac{\partial c(x, |p|)}{\partial x_i}. \quad (9)$$

151 Here δ_{ij} is Kronecker's delta, and c_y is the partial derivative of $c(x, y)$ with
 152 respect to the second variable.

153 As usual, for the sake of simplification of the presentation, we consider the
 154 case of spatially periodic boundary conditions [39] for Eqn. (7). Namely, we
 155 assume that there is an orthogonal basis $\{b_i\}$ in \mathbb{R}^n so that

$$u(\cdot, x) = u(\cdot, x + b_i), \quad x \in \mathbb{R}^n, \quad i = 1, \dots, n. \quad (10)$$

156 The problem is complemented with the initial condition

$$u(0, x) = u_0(x), \quad (11)$$

157 where $x \in \mathbb{R}^n$, and u_0 is Lipschitz and satisfies (10). Of course, c (and thus a
 158 and χ) should also satisfy the same spatial periodicity restriction (with respect
 159 to x but not to y or p).

160 Let us introduce the following algebraic notion. Given a diagonal matrix B ,
161 let $\text{mod}(B)$ be the matrix whose entries are the absolute values of the entries of
162 B . Furthermore, if B is an arbitrary symmetric matrix, it can be represented
163 as $Q^\top D Q$, where D is a diagonal matrix and Q is an orthogonal one. Then
164 we define $\text{mod}(B) = Q^\top \text{mod}(D) Q$. It is straightforward to check that this
165 definition does not depend on a particular choice of D and Q . Observe also that
166 $\text{mod}(B)$ is always positive-semidefinite, whereas $\text{mod}(B) = B$ when B itself is
167 positive-semidefinite.

168 We make the following assumptions:

a, χ are continuous, bounded, periodic in x , continuously differentiable in x , (12)

and their x -derivatives are uniformly (w.r.t. p) bounded, (13)

169

$$a_{ij}(x, p) \xi_i \xi_j \geq C \left[\text{mod} \left(\frac{\partial a(x, p)}{\partial x_k} \right) \right]_{ij} \xi_i \xi_j, \quad k = 1, \dots, n, \quad \xi, x, p \in \mathbb{R}^n, \quad (14)$$

$$g : \mathbb{R}^n \rightarrow \mathbb{R}, \quad 0 \leq g \leq 1, \quad \sqrt{g} \text{ is Lipschitz}, \quad (15)$$

170

$$G \in W_1^2(\mathbb{R}^n) \text{ (note that we do not assume it to be space-periodic)}, \quad (16)$$

171

$$\lambda \geq 0. \quad (17)$$

172 Here and below C stands for a generic positive constant, which can take different
173 values in different lines.

174 **Definition 1** (Viscosity solution). *A function u from the space*

$$C([0, T] \times \mathbb{R}^n) \cap L_\infty(0, T, W_\infty^1(\mathbb{R}^n)) \quad (18)$$

*is a viscosity sub-/supersolution to (7), (10), (11) if, for any $\phi \in C^2([0, T] \times \mathbb{R}^n)$
and any point $(t_0, x_0) \in (0, T] \times \mathbb{R}^n$ of local maximum/minimum of the function*

$u - \phi$, one has

$$\begin{aligned} \frac{\partial \phi(t_0, x_0)}{\partial t} - g((u * \nabla G)(t_0, x_0)) \operatorname{div}(c(x_0, |\nabla \phi(t_0, x_0)|) \nabla \phi(t_0, x_0)) \\ + \lambda(1 - g((u * \nabla G)(t_0, x_0)))(u(t_0, x_0) - u_0(x_0)) \leq 0 / \geq 0, \end{aligned} \quad (19)$$

175 and equalities (10), (11) hold in the classical sense. A viscosity solution is a
176 function which is both a subsolution and a supersolution.

177 3.2. Main result

178 **Theorem 1.** *i) The problem (7), (10), (11) has a viscosity solution in class*
179 *(18) for every positive T . Moreover,*

$$\inf_{\mathbb{R}^n} u_0 \leq u(t, x) \leq \sup_{\mathbb{R}^n} u_0. \quad (20)$$

180 *ii) Assume that*

$$\left| \left(\sqrt{a(x, p)} - \sqrt{a(z, p)} \right)_{ij} \right| \leq C|x - z|, \quad x, z, p \in \mathbb{R}^n. \quad (21)$$

181 Here $\sqrt{\cdot}$ is the square root of a positive-semidefinite symmetric matrix [41].
182 Then the solution is unique. Moreover, for any two viscosity solutions u and v
183 to (7), the following estimate holds

$$\sup_{\mathbb{R}^n} |u(t, \cdot) - v(t, \cdot)| \leq \Phi(t) \sup_{\mathbb{R}^n} |u(0, \cdot) - v(0, \cdot)| \quad (22)$$

184 with some non-decreasing continuous scalar function Φ dependent on u and v .

185 *Proof.* Note that (20) is a direct consequence of the definition of viscosity
186 solution: to get the second inequality, one can put $\phi(t, x) = \delta t$, then, at
187 the point (t_0, x_0) , $t_0 > 0$, of the global maximum of $u(t, x) - \delta t$, (19) gives
188 $\delta + \lambda(1 - g((u * \nabla G)(t_0, x_0)))(u(t_0, x_0) - u_0(x_0)) \leq 0$, whence $u(t_0, x_0) < u_0(x_0)$,
189 so we get a contradiction since $u(t_0, x_0) - \delta t_0 \geq u_0(x_0)$ due to the fact that
190 (t_0, x_0) is the global maximum point of $u(t, x) - \delta t$; thus the function $u(t, x) - \delta t$
191 attains its global maximum at $t = 0$, and it remains to let $\delta \rightarrow +0$; similarly
192 one derives the first one.

Now, we establish a *formal a priori estimate* for $\sup_{\mathbb{R}^n} |\nabla u|$. Observe that (7) is equivalent to

$$\begin{aligned} \frac{\partial u}{\partial t} &= g(u * \nabla G) [a_{ij}(x, \nabla u) u_{x_i x_j} + \chi_i(x, \nabla u) u_{x_i}] \\ &\quad - \lambda(1 - g(u * \nabla G))(u - u_0). \end{aligned} \quad (23)$$

Fix T . Differentiating (23) with respect to each x_k , $k = 1, \dots, n$, multiplying by $2u_{x_k}$, and adding the results, we get

$$\begin{aligned} \mathcal{L}(|\nabla u|^2) &:= \frac{\partial |\nabla u|^2}{\partial t} - g a_{ij}(x, \nabla u) \frac{\partial^2}{\partial x_i \partial x_j} |\nabla u|^2 \\ &\quad - g \frac{\partial a_{ij}(x, \nabla u)}{\partial p_l} u_{x_i x_j} \frac{\partial}{\partial x_l} |\nabla u|^2 \\ &\quad - g \chi_i(x, \nabla u) \frac{\partial}{\partial x_i} |\nabla u|^2 - g \frac{\partial \chi_i(x, \nabla u)}{\partial p_l} u_{x_i} \frac{\partial}{\partial x_l} |\nabla u|^2 \\ &= -2g a_{ij}(x, \nabla u) u_{x_k x_i} u_{x_k x_j} + 2\nabla g(u * \nabla G) \cdot \left(u * \frac{\partial \nabla G}{\partial x_k} \right) a_{ij}(x, \nabla u) u_{x_i x_j} u_{x_k} \\ &\quad + 2g \frac{\partial a_{ij}(x, \nabla u)}{\partial x_k} u_{x_i x_j} u_{x_k} + 2\nabla g(u * \nabla G) \cdot \left(u * \frac{\partial \nabla G}{\partial x_k} \right) \chi_i(x, \nabla u) u_{x_i} u_{x_k} \\ &\quad + 2g \frac{\partial \chi_i(x, \nabla u)}{\partial x_k} u_{x_i} u_{x_k} - 2\lambda(1 - g) u_{x_k} u_{x_k} + 2\lambda(1 - g) (u_0)_{x_k} u_{x_k} \\ &\quad + 2\lambda \nabla g(u * \nabla G) \cdot \left(u * \frac{\partial \nabla G}{\partial x_k} \right) (u - u_0) u_{x_k}. \end{aligned} \quad (24)$$

193 At this point, we need the following generalization of [39, Lemma 2.6].

194 **Lemma 1.** *Let A and B be quadratic matrices of order n . Assume that B is*
195 *symmetric, and there is a constant $M \geq 0$ such that*

$$M A_{ij} \xi_i \xi_j \geq \text{mod}(B)_{ij} \xi_i \xi_j, \quad \forall \xi \in \mathbb{R}^n. \quad (25)$$

196 *Then for any matrix U (of the same order but not necessarily symmetric) one*
197 *has*

$$\text{Tr}^2(BU^\top) \leq M \|B\| \text{Tr}(UAU^\top), \quad (26)$$

198 *where $\|\cdot\|$ denotes the operator norm of a matrix.*

Proof. Formulas (25) and (26) are invariant with respect to orthogonal changes of bases. Thus, without loss of generality we may assume that B is already

diagonalized by an orthogonal transform. Then

$$\begin{aligned}
Tr^2(BU^\top) &= (B_{ii}U_{ii})^2 \leq \|B\| \|B_{ii}\| U_{ii}^2 \\
&= \|B\| (mod(B))_{ii} U_{ii}^2 \leq \|B\| (mod(B))_{ii} U_{ki} U_{ki} \\
&= \|B\| (mod(B))_{ij} U_{ki} U_{kj} \leq M \|B\| A_{ij} U_{ki} U_{kj} = M \|B\| Tr(UAU^\top).
\end{aligned}$$

199

□

This lemma gives opportunity to discharge the undesired influence of the second and the third terms in the right-hand side of (24). For the third one, due to the lemma, (14) and Cauchy's inequality, we have

$$\begin{aligned}
\left| 2g \frac{\partial a_{ij}(x, \nabla u)}{\partial x_k} u_{x_i x_j} u_{x_k} \right| &\leq Cg |u_{x_k}| \sqrt{a_{ij}(x, \nabla u) u_{x_k x_i} u_{x_k x_j}} \\
&\leq g a_{ij}(x, \nabla u) u_{x_k x_i} u_{x_k x_j} + C|\nabla u|^2. \quad (27)
\end{aligned}$$

200 Since our assumptions yield

$$\left| u * \frac{\partial \nabla G}{\partial x_k} \right| \leq C, \quad (28)$$

201 and

$$|\nabla g| \leq C\sqrt{g}, \quad (29)$$

an application of the lemma with $A = B = a$ and $M = 1$ implies

$$\begin{aligned}
\left| 2\nabla g(u * \nabla G) \cdot \left(u * \frac{\partial \nabla G}{\partial x_k} \right) a_{ij}(x, \nabla u) u_{x_i x_j} u_{x_k} \right| \\
\leq C |u_{x_k}| \sqrt{g a_{ij}(x, \nabla u) u_{x_k x_i} u_{x_k x_j}} \\
\leq g a_{ij}(x, \nabla u) u_{x_k x_i} u_{x_k x_j} + C|\nabla u|^2. \quad (30)
\end{aligned}$$

202 The sum of the absolute values of the subsequent terms of the right-hand
203 side of (24) does not exceed $C(1 + |\nabla u|^2)$. Thus,

$$\mathcal{L}(|\nabla u|^2) \leq C(1 + |\nabla u|^2), \quad (31)$$

204 SO

$$\mathcal{L}(e^{-Ct}(1 + |\nabla u|^2)) \leq 0. \quad (32)$$

205 From the weak maximum principle for the weakly parabolic operator \mathcal{L} one
 206 easily concludes that

$$|\nabla u|^2 \leq C. \quad (33)$$

207 Using (20) and (33), by means of the approach from [39] we can get the
 208 uniform Hölder estimate

$$|u(t, x) - u(s, x)|^2 \leq C|t - s|. \quad (34)$$

209 Then, following [43, 39], we approximate our problem by well-posed ones in
 210 the sense of [42, Chapter 5]. Due to (20), (33) and (34), the solutions of these
 211 problems are uniformly bounded and equicontinuous on $[0, T] \times \mathbb{R}^n$. Then we
 212 can select a uniformly converging sequence of approximate solutions, and pass
 213 to the limit in the viscosity sense using the general consistency/stability results
 214 from [40]. The uniqueness of solutions follows from the stability estimate (22).
 215 This bound may be shown by revisiting the proof of a similar bound in [43, 39].
 216 We only point out that the matrix Γ [39, p. 159] is replaced by

$$\Gamma_* = \begin{pmatrix} g_1 \Lambda_1 & \sqrt{g_1 g_2} \sqrt{\Lambda_1} \sqrt{\Lambda_2} \\ \sqrt{g_1 g_2} \sqrt{\Lambda_2} \sqrt{\Lambda_1} & g_2 \Lambda_2 \end{pmatrix}, \quad (35)$$

where

$$\Lambda_1 = a \left(x_0, \frac{|x_0 - y_0|^2 (x_0 - y_0)}{\varepsilon} \right), \quad \Lambda_2 = a \left(y_0, \frac{|x_0 - y_0|^2 (x_0 - y_0)}{\varepsilon} \right),$$

217 and the notation within is taken from [39]. Note that the $2n \times 2n$ -matrix Γ_* is
 218 symmetric and positive-semidefinite.

219 □

220 4. Numerical Results

221 4.1. Comparison with other schemes

222 The proposed scheme is compared with related diffusion based denoising
 223 schemes from the literature. To make a fair comparison we utilize the same
 224 diffusion function c_{pm1} from (3) in all the compared schemes and the contrast

225 parameter K is fixed using the original criteria given in [1], see [44, 45] for
 226 other choices. Moreover, the edge stopping function $g(\xi) = (1 + |\xi|)^{-1}$ is fixed
 227 wherever applicable and the classical fidelity term is utilized unless otherwise
 228 stated.

229 (a) Perona and Malik [1] - Anisotropic Diffusion (AD) Eqn. (2) with c_{pm1}
 230 in (3):

$$\frac{\partial u}{\partial t} = \operatorname{div} \left(\frac{\nabla u}{1 + |\nabla u|^2 / K^2} \right)$$

231 (b) Catté et al [8] - Smoothed Gradient based anisotropic diffusion (SG) with
 232 c_{pm1} in (3):

$$\frac{\partial u}{\partial t} = \operatorname{div} \left(\frac{\nabla u}{1 + |\nabla G_\sigma \star u|^2 / K^2} \right)$$

233 (c) Rudin et al [32] - Total Variation (TV) (2) with $c(s) = (\epsilon + s^2)^{-1/2}$,
 234 $\epsilon = 10^{-6}$:

$$\frac{\partial u}{\partial t} = \operatorname{div} \left(\frac{\nabla u}{\sqrt{\epsilon + |\nabla u|^2}} \right)$$

235 (d) El Falah and Ford [29] - Mean Curvature Motion (MCM), Eqn. (4) with
 236 $\lambda = 0$:

$$\frac{\partial u}{\partial t} = \frac{1}{1 + |\nabla u|^2} \operatorname{div} \left(\frac{\nabla u}{1 + |\nabla u|^2 / K^2} \right)$$

237 (e) Barcelos et al [27] - Well-Balanced Flow (WBF):

$$\frac{\partial u}{\partial t} = g(|\nabla G_\sigma \star u|) \operatorname{div} \left(\frac{\nabla u}{1 + |\nabla u|^2 / K^2} \right) - \lambda(1 - g(|\nabla G_\sigma \star u|))(u - u_0)$$

238 (f) Shi and Chang [9] - Modified Smoothed Gradient based anisotropic diffu-
 239 sion (MSG):

$$\frac{\partial u}{\partial t} = |\nabla G_\sigma \star u| \operatorname{div} \left(\frac{\nabla G_\sigma \star u}{|\nabla G_\sigma \star u|} \right) - |\nabla G_\sigma \star u| \lambda(G_\sigma \star u - u_0)$$

240 Further, similar adaptive schemes which utilize different diffusion coefficient
 241 functions are also compared.

242 (a) Weickert [46] - Edge Enhancing Diffusion (EED):

243 PM PDE (2) with the diffusion function:

$$c(|\nabla u|) = \begin{cases} \exp(-0.234 |\nabla u|) & \text{if } |\nabla u| \geq K \\ 0 & \text{if } |\nabla u| < K \end{cases}$$

244 (b) Weickert [47] - Coherence Enhancing Diffusion (CED):

245 PM PDE (2) with the diffusion function constructed using the structure
246 tensor, see [47] for more details. The eigenvalues of D are chosen as, for
247 μ_1, μ_2 eigenvalues of the structure tensor, $\alpha \in (0, 1)$, $C > 0$: $\lambda_1 = \alpha$, and

$$\lambda_2 = \begin{cases} \alpha & \text{if } \mu_1 = \mu_2 \\ \alpha + (1 - \alpha) \exp\left(\frac{-C}{(\mu_1 - \mu_2)^2}\right) & \text{else} \end{cases}$$

248 (c) Kačur and Mikula [48, 35] - Slowed Anisotropic Diffusion (SAD):

$$\frac{\partial u}{\partial t} = \operatorname{div} \left(\frac{\nabla G_\sigma \star u}{1 + |\nabla G_\sigma \star u|^2 / K^2} \nabla \beta(x, u) \right)$$

249 with $\beta(x, u) = 0$ for $u \in [0, 0.5]$ and $\beta(x, u) = u$ for $u \in (0.5, 1]$.

250 (d) Strong [16] - Adaptive TV (ATV):

$$\frac{\partial u}{\partial t} = \operatorname{div} \left(\frac{\alpha(x) \nabla u}{\sqrt{\epsilon + |\nabla u|^2}} \right)$$

251 with $\alpha(x) = (1 + |\nabla u_0|)^{-1}$, $\epsilon = 10^{-6}$.

252 (e) Kusnezow et al [19] - Adaptive Linear Diffusion (ALD):

$$\frac{\partial u}{\partial t} = \alpha \operatorname{div} (\nabla u)$$

253 with $\alpha = (1 + M_c \chi_c)$, $M_c \gg 0$ constant and χ_c is a smooth edge indicator
254 function.

255 (f) Prasath and Singh [22] - Edge detector based Anisotropic Diffusion (EAD)

$$\frac{\partial u}{\partial t} = \operatorname{div} \left(\frac{\alpha(x) \nabla u}{1 + |\nabla u|^2 / K^2} \right)$$

256 with $\alpha(x) = 1 - G_\sigma \star C(u(x, t))$, C - Canny edge detector output.

257 In the comparison results, apart from using the proposed adaptive fidelity term
 258 based WWBF (see Eqn. (6) and Section 2.3),

$$\frac{\partial u(x, t)}{\partial t} = g \operatorname{div} (c(x, |\nabla u|) \nabla u(x, t)) - \lambda(1 - g)(u(x, t) - u(x, t - 1)),$$

259 we also utilize the weighted Linear Diffusion (WLD) - using the proposed weight
 260 in a linear diffusion framework,

$$\frac{\partial u}{\partial t} = g \operatorname{div} (\alpha(x) \nabla u) - \lambda(1 - g)(u(x, t) - u(x, t - 1)).$$

261 4.2. Implementation details

262 The additive operator splitting (AOS) scheme which is proven to be effective
 263 in diffusion PDE based image processing [7] is used to implement the schemes.
 264 The images were scaled to the interval $[0, 1]$. It can be described briefly as
 265 follows: In 1-D with matrix-vector notation, the iterative scheme is,

$$U^{t+1} = [1 - \tau A(U^t)]^{-1} U^t,$$

266 where τ is the time step, $A(U^t) = [a_{ij}(U^t)]$, and

$$a_{ij}(U^t) := \begin{cases} \frac{\gamma_i^t + \gamma_j^t}{2h^2} & j \in \mathcal{N}_i \\ -\sum_{k \in \mathcal{N}_i} \frac{\gamma_i^t + \gamma_k^t}{2h^2} & j = i \\ 0 & \text{otherwise} \end{cases}$$

267 with $\gamma_i = \alpha_i g_i$ and h discretization step size. For n-D images the semi-implicit
 268 scheme is written as

$$U^{t+1} = \left[1 - \tau \sum_{l=1}^n A_l(U^t) \right]^{-1} U^t. \quad (36)$$

269 The matrix $A_l = (a_{ijl})_{ij}$ corresponds to derivatives along the l -th coordinate
 270 axis.

271 **Remark 3.** *The spatial step size $h = 1$ is fixed as the pixel grid has the natural*
 272 *spacing of size one. Further the time step $\tau = 0.2$, pre-smoothing parameter*
 273 *$\sigma = 1$, and fidelity parameter $\lambda = 1$ are fixed for all the experiments reported*
 274 *here.*

275 **Remark 4.** Under the AOS type discretization (36), the proposed WWBF
 276 scheme (6) satisfies the usual scale space properties, see [7] for more details.
 277 Moreover the maximum-minimum principle also holds, see Theorem 1.

278 4.3. Visual comparison

279 Figure 4 shows the comparison of non-adaptive diffusion schemes based
 280 restoration results for a noisy (Gaussian noise, $\sigma_n = 25$) *Lena* gray-scale image.
 281 In each pair, left image shows the 156×156 crop of the restored image and
 282 the right image shows the contour view to highlight the movement of level-sets
 283 under different schemes. Note that, the proposed approach gives better result
 284 even with linear diffusion, see Figure 4(g) which corresponds to WLD scheme
 285 result. As can be seen by comparing the contour maps of each scheme, the
 286 proposed scheme's result in Figure 4(h) gives better result in terms denoising
 287 as well as staircasing artifact free restoration.

288 To compare the adaptive diffusion schemes in a fair manner we utilize a test
 289 image synthetically generated consist of a slope, strong edges and a circle with
 290 oscillations. Figure 5 shows the comparison results for the noisy *Kikis* image
 291 ($\sigma_n = 30$ is added to the original image, see Figure 1(d)) by different adaptive
 292 diffusion schemes. The Perona-Malik, TV based schemes such as EED, CED,
 293 SAD, ATV inherit the original staircasing artifacts whereas WWBF performs
 294 better than other schemes in terms of edge preservation without oscillations, see
 295 Figure 5(h).

296 Finally, to show the effect of the adaptive fidelity term in different adaptive
 297 schemes we perform experiments on a synthetic *Circles* gray-scale image which
 298 has multiple circular regions with different piecewise constant regions. Figure 6
 299 shows the comparison of the adaptive schemes SAD, ATV, ALD, and EAD
 300 with the same adaptive fidelity chosen as in our WWBF scheme, i.e., $(u(x, t) -$
 301 $u(x, t - 1))$. As can be seen the WWBF scheme preserves edges without any
 302 blocky artifacts. Moreover, the adaptive fidelity term captures the circular
 303 edges thereby balances the adaptive diffusion near the edges. Supplementary
 304 MATLAB .fig files are provided to show 3D visualizations of resultant images

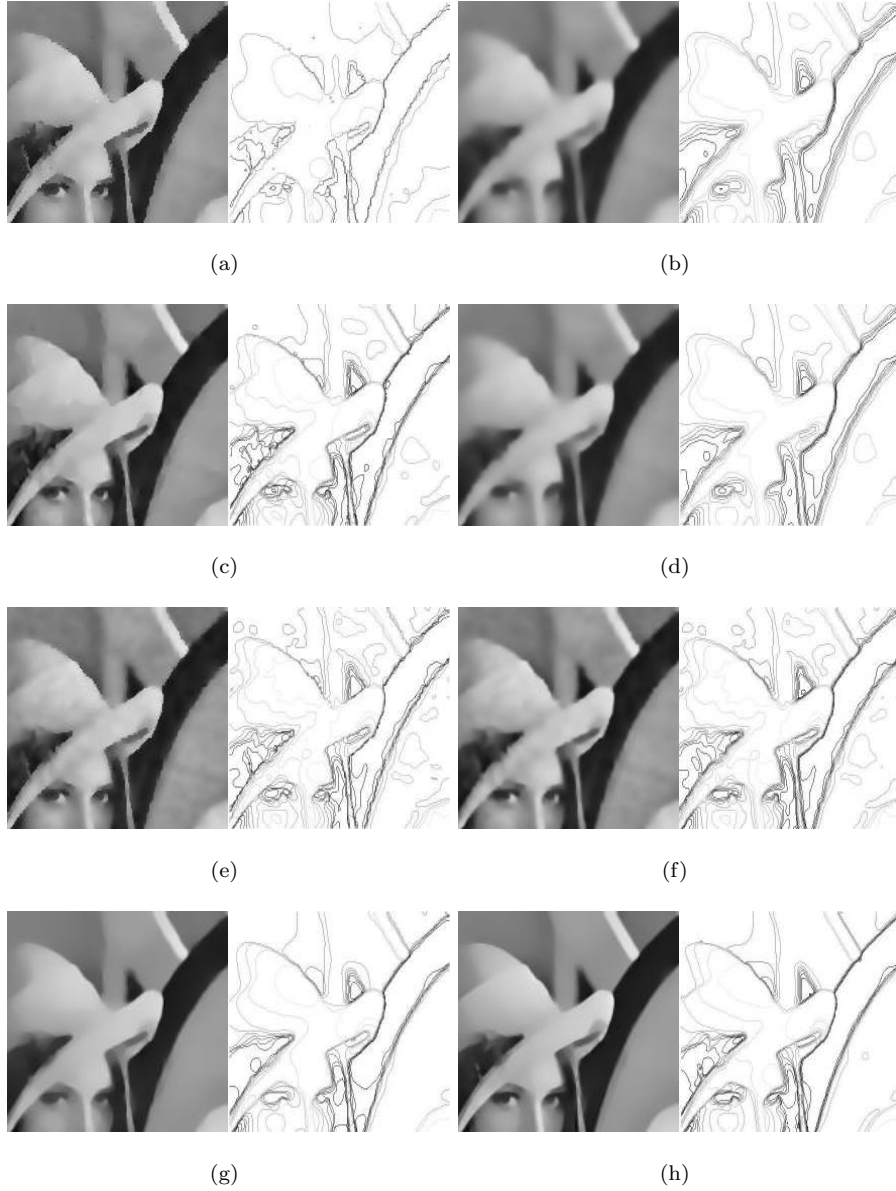


Figure 4: Comparison results for *Lena* image, cropped 156×156 image (in each sub-figure, the right image shows the contour view of the left image). (a) AD [1] (b) SG [8] (c) TV [32] (d) MCM [29] (e) WBF [27] (f) MSG [9] (g) Proposed scheme with linear diffusion (WLD) (h) Proposed scheme with nonlinear diffusion (WWBF).

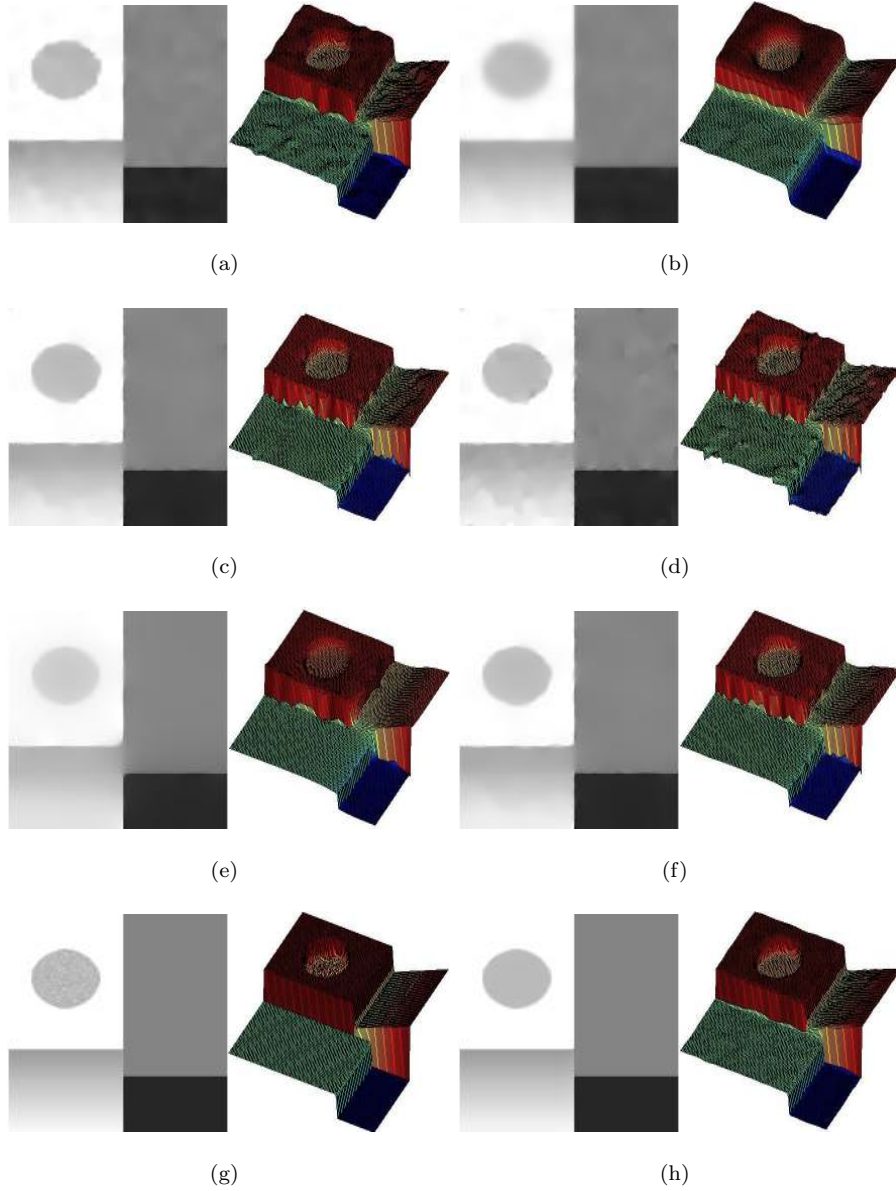


Figure 5: Adaptive schemes comparison results on *Kikis* 128×128 synthetic image, (in each sub-figure, the right image shows the surface form of the left image): (a) EED [46] (b) CED [47] (c) SAD [48] (d) ATV [16] (e) ALD [19] (f) EAD [22] (g) Original image and its surface form given for comparison (h) Proposed scheme with nonlinear diffusion (WWBF).

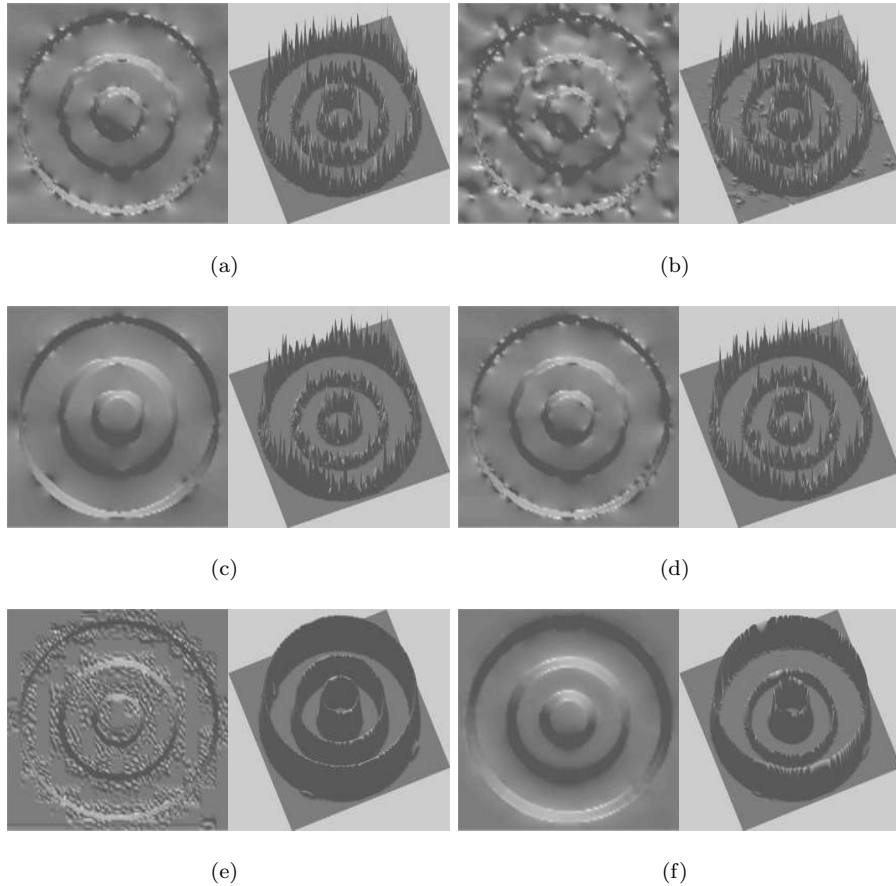


Figure 6: Adaptive schemes comparison results on *Circles* 120×120 synthetic image, (in each sub-figure, right image shows the resultant and left image adaptive fidelity term at the final iteration in surface format): (a) SAD [48] (b) ATV [16] (c) ALD [19] (d) EAD [22] (e) Original image and its edge map given in surface format for comparison. Note that artifacts are due to jpeg compression which appear near edges. (f) Proposed scheme with nonlinear diffusion (WWBF). Supplementary MATLAB .fig files are provided to show 3D visualizations of resultant images shown here.

305 shown on the left of each sub-figure.

306 **Remark 5.** *Other non-adaptive diffusion schemes such as AD, SG, TV, MCM,*
 307 *WBF, MSG and directional diffusion models such as EED, CED do not utilize*
 308 *an adaptive weight as in our case (see Eqn. (5)). Moreover, the adaptive data*
 309 *fidelity term did not provide any visually improved denoising results for these*
 310 *schemes, hence we omit the images in Figure 6 for brevity.*

311 4.4. Quantitative comparison and discussion

312 To compare the schemes quantitatively we utilize two commonly used error
 313 metrics in the image denoising literature, one is the classical peak signal to
 314 noise ratio (PSNR) [2], and the other is the mean structural similarity measure
 315 (MSSIM) [49]:

- 316 1. PSNR is given in decibels (dB). A difference of $0.5 dB$ can be identified
 317 visually. Higher PSNR value indicates optimum denoising capability.

$$\text{PSNR}(u) := 20 * \log_{10} \left(\frac{u_{max}}{\sqrt{MSE}} \right) dB$$

318 where $MSE = (mn)^{-1} \sum \sum (u - u_0)$, $m \times n$ denotes the image size, u_{max}
 319 denotes the maximum value, for example in 8-bit images $u_{max} = 255$.

- 320 2. MSSIM index is in the range $[0, 1]$. The MSSIM value near one implies
 321 the optimal denoising capability of the scheme [49] and is mean value of
 322 the SSIM metric. The SSIM is calculated between two windows ω_1 and
 323 ω_2 of common size $N \times N$,

$$\text{SSIM}(\omega_1, \omega_2) = \frac{(2\mu_{\omega_1}\mu_{\omega_2} + c_1)(2\sigma_{\omega_1\omega_2} + c_2)}{(\mu_{\omega_1}^2 + \mu_{\omega_2}^2 + c_1)(\sigma_{\omega_1}^2 + \sigma_{\omega_2}^2 + c_2)}$$

324 where μ_{ω_i} the average of ω_i , $\sigma_{\omega_i}^2$ the variance of ω_i , $\sigma_{\omega_1\omega_2}$ the covariance,
 325 c_1, c_2 stabilization parameters, see [49] for more details.

326 Table 2 shows the comparison results using these two metrics for all schemes
 327 without data adaptive fidelity term. Corresponding PSNR and MSSIM values
 328 are given for each of the schemes and clearly our scheme performs better than
 329 or on par with other diffusion schemes in general. We also include comparison

330 results with corresponding data adaptive fidelity term described in Section 2.3.
331 As can be noted, the proposed scheme performs well for a variety of images
332 (taken from the standard test images USC-SIPI database) for both data fidelity
333 versions. Note that the PSNR values are closer together when adaptive fidelity
334 is used (SAD, ATV, ALD, EAD, and our WWBF) in Table 2, but MSSIM values
335 indicate a better performance of the proposed approach. Thus, the proposed
336 adaptive WWBF flow preserves salient structures (edges) when compared with
337 other nonlinear heat diffusion flows. The *Baboon* image consist of texture parts
338 and hence the proposed WWBF scheme can not obtain optimal PSNR/MSSIM
339 values. To alleviate this a spatially adaptive fidelity parameter $\lambda = \lambda(x)$ can be
340 incorporated, see Section 2.3. Following [28] automatic selection of parameters
341 is one of the current research being carried out. Moreover, the image restoration
342 model studied here can be used in other image processing algorithms such as
343 inpainting [50, 51] and edge detection [27] as well.

344 5. Conclusions

345 Well-balanced flow is based on a nonlinear diffusion PDE which is utilized
346 in image noise removal and edge detection successfully. In this paper, a new
347 variant of the flow is considered by using weights in the divergence diffusion pro-
348 cess. This improves the denoising capabilities as well as the multi-scale detail
349 preservation of the corresponding PDE. Numerical experiments on noisy images
350 shows the proposed scheme's performs well on a variety of images. Extensive ex-
351 periments indicate the improvements over other classical diffusion and adaptive
352 diffusion schemes.

353 Acknowledgement

354 The authors would like to thank the anonymous referees for their construc-
355 tive comments which improved the paper considerably. Part of this work was
356 done while the first author was visiting Institute for Pure and Applied Mathe-
357 matics (IPAM), University of California Los Angeles (UCLA), USA. The first

Table 2: PSNR (dB) and MSSIM comparison for standard test images with and without adaptive fidelity term for different diffusion based schemes. Noisy image is obtained by adding Gaussian noise of strength $\sigma_n = 25$ to the original image of size 256×256 except for the image *Kikis* which has $\sigma_n = 30$ and size 128×128 . Each row indicates the PSNR/MSSIM values for different test images. Overline indicate the PDE is used with adaptive data-fidelity and best results are indicated by boldface.

Scheme	Ref.	<i>Kikis</i>	<i>Lena</i>	<i>House</i>	<i>Peppers</i>	<i>Baboon</i>
Noisy		18.56/0.1683	20.14/0.3866	20.14/0.2732	20.14/0.3426	20.14/0.4643
AD	[1]	33.32/0.9081	26.32/0.7752	28.87/0.8300	27.37/0.8170	23.48/0.4687
SG	[8]	29.09/0.9036	23.26/0.6708	24.94/0.7657	23.09/0.7291	22.35/0.3653
TV	[32]	33.47/0.9414	27.05/0.7951	30.18/0.8520	28.30/0.8389	23.61/0.4899
MCM	[29]	30.87/0.9238	23.97/0.6943	25.89/0.7855	24.02/0.7501	22.44/0.3723
WBF	[27]	33.19/0.9111	26.46/0.7827	28.94/0.8286	27.63/0.8289	23.54/0.4802
MSG	[9]	33.23/0.9273	26.53/0.7826	29.30/0.8370	27.31/0.8327	23.34/0.4627
EED	[46]	35.23/0.9530	27.23/0.7980	30.68/0.8554	28.44/ 0.8435	23.47/0.4685
CED	[47]	30.87/0.9238	23.97/0.6943	25.89/0.7855	24.02/0.7501	22.44/0.3723
SAD	[48]	34.57/0.9593	25.85/0.7559	29.18/0.8375	26.93/0.8030	22.90/0.4133
ATV	[16]	33.68/0.9435	27.26/0.7972	30.39/0.8541	28.51/0.8410	23.82 /0.4920
ALD	[19]	28.48/0.9378	20.70/0.5965	23.23/0.7346	20.58/0.6248	20.84/0.3105
EAD	[22]	34.24/0.9600	24.88/0.7247	28.17/0.8221	25.72/0.7719	22.47/0.3762
WLD		32.81/0.9423	23.87/0.7126	27.03/0.8088	23.91/0.7306	20.73/0.3557
WWBF		37.00/0.9499	27.12/0.7815	30.92/0.8584	28.27/0.8109	22.98/0.4417
$\overline{\text{SAD}}$		34.45/0.9601	24.05/0.7595	27.82/0.8409	24.36/0.8109	20.00/0.4211
$\overline{\text{ATV}}$		30.96/0.9481	24.69/ 0.8028	28.93/0.8581	26.09/0.8483	22.67/ 0.5004
$\overline{\text{ALD}}$		26.09/0.9407	19.58/0.6053	21.36/0.7562	18.84/0.6490	19.08/0.3279
$\overline{\text{EAD}}$		33.78/0.9658	22.80/0.7203	26.77/0.8339	24.96/0.7740	21.58/0.3836
$\overline{\text{WLD}}$		33.71/0.9652	24.90/0.7269	28.63/0.8293	25.77/0.7692	22.40/0.3693
$\overline{\text{WWBF}}$		38.54/0.9696	27.42 /0.7965	31.27/0.8621	28.73 /0.8356	23.46/0.4533

358 author thanks the IPAM institute for their great hospitality and support during
359 the visit. The second author was supported by CMUC (University of Coimbra)
360 and FCT (Portugal), and through European program COMPETE/FEDER.

361 References

- 362 [1] P. Perona, J. Malik, Scale-space and edge detection using anisotropic dif-
363 fusion, *IEEE Transactions on Pattern Analysis and Machine Intelligence*
364 12 (7) (1990) 629–639. doi:10.1109/34.56205.
- 365 [2] G. Aubert, P. Kornprobst, *Mathematical problems in image processing:*
366 *Partial differential equation and calculus of variations*, Springer-Verlag,
367 New York, USA, 2006.
- 368 [3] S. Kichenassamy, The Perona-Malik paradox, *SIAM Journal on Applied*
369 *Mathematics* 57 (5) (1997) 1328–1342. doi:10.1137/S003613999529558X.
- 370 [4] Y.-L. You, W. Xu, A. Tannenbaum, M. Kaveh, Behavioral analysis of
371 anisotropic diffusion in image processing, *IEEE Transactions on Image Pro-*
372 *cessing* 5 (11) (1996) 1539–1553. doi:10.1109/83.541424.
- 373 [5] C. A. Z. Barcelos, Y. Chen, Heat flows and related minimization problem in
374 image restoration, *Computers & Mathematics with Applications* 39 (5–6)
375 (2000) 81–97. doi:10.1016/S0898-1221(00)00048-1.
- 376 [6] T. Barbu, V. Barbu, V. Biga, D. Coca, A PDE variational approach to
377 image denoising and restoration, *Nonlinear Analysis: Real World Applica-*
378 *tions* 10 (3) (2009) 1351–1361. doi:10.1016/j.nonrwa.2008.01.017.
- 379 [7] J. Weickert, B. M. H. Romeny, M. A. Viergever, Efficient and reliable
380 schemes for nonlinear diffusion filtering, *IEEE Transactions on Image Pro-*
381 *cessing* 7 (3) (1998) 398–410. doi:10.1109/83.661190.
- 382 [8] V. Catte, P. L. Lions, J.-M. Morel, T. Coll, Image selective smoothing and
383 edge detection by nonlinear diffusion, *SIAM Journal on Numerical Analysis*
384 29 (1) (1992) 182–193. doi:10.1137/0729012.

- 385 [9] Y. Shi, Q. Chang, New time dependent model for image restoration,
386 Applied Mathematics and Computation 179 (1) (2006) 121–134. doi:
387 [10.1016/j.amc.2005.11.085](https://doi.org/10.1016/j.amc.2005.11.085).
- 388 [10] H. Amann, Time-delayed Perona-Malik type problems, Acta Mathematica
389 Universitatis Comenianae LXXVI (1) (2007) 15–38.
- 390 [11] E. Tadmor, P. Athavale, Multiscale image representation using novel
391 integro-differential equations, Inverse Problems and Imaging 3 (4) (2009)
392 693–710. doi:[10.3934/ipi.2009.3.693](https://doi.org/10.3934/ipi.2009.3.693).
- 393 [12] M. Nitzberg, T. Shiota, Nonlinear image filtering with edge and corner
394 enhancement, IEEE Transactions on Pattern Analysis and Machine Intel-
395 ligence 14 (8) (1992) 826–833. doi:[10.1109/34.149593](https://doi.org/10.1109/34.149593).
- 396 [13] Y. Chen, C. A. Z. Barcelos, B. A. Mair, Smoothing and edge detection
397 by time-varying coupled nonlinear diffusion equations, Computer Vision
398 and Image Understanding 82 (2) (2001) 85–100. doi:[10.1006/cviu.2001.](https://doi.org/10.1006/cviu.2001.0903)
399 [0903](https://doi.org/10.1006/cviu.2001.0903).
- 400 [14] A. Belahmidi, A. Chambolle, Time-delay regularization of anisotropic dif-
401 fusion and image processing, Mathematical Modelling and Numerical Anal-
402 ysis 39 (2) (2005) 231–251. doi:[10.1051/m2an:2005010](https://doi.org/10.1051/m2an:2005010).
- 403 [15] V. B. S. Prasath, D. Vorotnikov, On a system of adaptive coupled pdes
404 for image restoration, Journal of Mathematical Imaging and Vision Online
405 First, available at arXiv:1112.2904. doi:[10.1007/s10851-012-0386-3](https://doi.org/10.1007/s10851-012-0386-3).
- 406 [16] D. Strong, Adaptive total variation minimizing image restoration, Ph.D.
407 thesis, UCLA Mathematics Department, USA (August 1997).
- 408 [17] Y. Chen, T. Wunderli, Adaptive total variation for image restoration in BV
409 space, Journal of Mathematical Analysis and Applications 272 (3) (2002)
410 117–137. doi:[10.1016/S0022-247X\(02\)00141-5](https://doi.org/10.1016/S0022-247X(02)00141-5).

- 411 [18] Y. Chen, S. Levine, M. Rao, Variable exponent, linear growth functionals
412 in image restoration, *SIAM Journal on Applied Mathematics* 66 (4) (2006)
413 1383–1406. doi:10.1137/050624522.
- 414 [19] W. Kusnezow, W. Horn, R. P. Wurtz, [Fast image processing with con-](#)
415 [straints by solving linear PDEs](#), *Electronic Letters on Computer Vision*
416 *and Image Analysis* 6 (2) (2007) 22–35, special Issue: Partial Differential
417 Equations Methods in Graphics and Vision.
418 URL <http://elcvia.uab.es/index.php/elcvia/article/view/146>
- 419 [20] R. Aboulaich, D. Meskine, A. Souissi, New diffusion models in image pro-
420 cessing, *Computers & Mathematics with Applications* 56 (4) (2008) 874–
421 882. doi:10.1016/j.camwa.2008.01.017.
- 422 [21] V. B. S. Prasath, A. Singh, A hybrid convex variational model for image
423 restoration, *Applied Mathematics and Computation* 215 (10) (2010) 3655–
424 3664. doi:10.1016/j.amc.2009.11.003.
- 425 [22] V. B. S. Prasath, A. Singh, Well-posed inhomogeneous nonlinear diffusion
426 scheme for digital image denoising, *Journal of Applied Mathematics* 2010
427 (2010) 14pp, article ID 763847. doi:10.1155/2010/763847.
- 428 [23] P. Guidotti, A new nonlocal nonlinear diffusion of image processing, *Journal*
429 *of Differential Equations* 246 (12) (2009) 4731–4742. doi:10.1016/j.jde.
430 2009.03.017.
- 431 [24] P. Guidotti, J. Lambers, Two new nonlinear nonlocal diffusions for noise
432 reduction, *Journal of Mathematical Imaging Vision* 33 (1) (2009) 25–37.
433 doi:10.1007/s10851-008-0108-z.
- 434 [25] P. Guidotti, A new well-posed nonlinear nonlocal diffusion, *Nonlinear*
435 *Analysis: Theory, Methods & Applications* 72 (12) (2010) 4625–4637.
436 doi:10.1016/j.na.2010.02.040.

- 437 [26] P. Guidotti, K. Longo, Two enhanced fourth order diffusion models for
438 image denoising, *Journal of Mathematical Imaging Vision* 40 (2) (2011)
439 188–198. [doi:10.1007/s10851-010-0256-9](https://doi.org/10.1007/s10851-010-0256-9).
- 440 [27] C. A. Z. Barcelos, M. Boaventura, E. Silva Jr, A well-balanced flow equa-
441 tion for noise removal and edge detection, *IEEE Transactions on Image*
442 *Processing* 12 (7) (2003) 751–763. [doi:10.1109/TIP.2003.814242](https://doi.org/10.1109/TIP.2003.814242).
- 443 [28] C. A. Z. Barcelos, M. Boaventura, E. Silva Jr, Edge detection and noise
444 removal by use of a partial differential equation with automatic selection of
445 parameters, *Computational & Applied Mathematics* 24 (1) (2005) 131–150.
- 446 [29] A. I. El-Fallah, G. E. Ford, On mean curvature diffusion in nonlinear image
447 filtering, *Pattern Recognition Letters* 19 (5–6) (1998) 433–437. [doi:10.](https://doi.org/10.1016/S0167-8655(98)00030-0)
448 [1016/S0167-8655\(98\)00030-0](https://doi.org/10.1016/S0167-8655(98)00030-0).
- 449 [30] K. N. Nordstrom, Biased anisotropic diffusion: a unified regularization and
450 diffusion approach to edge detection, *Image and Vision Computing* 8 (4)
451 (1990) 318–327. [doi:10.1016/0262-8856\(90\)80008-H](https://doi.org/10.1016/0262-8856(90)80008-H).
- 452 [31] B. Smolka, Modified biased anisotropic diffusion processing of noisy color
453 images, in: *Ninth IEEE International Conference on Signal Processing*,
454 Beijing, China, 2008, pp. 777–780. [doi:10.1109/ICOSP.2008.4697245](https://doi.org/10.1109/ICOSP.2008.4697245).
- 455 [32] L. Rudin, S. Osher, E. Fatemi, Nonlinear total variation based noise re-
456 moval algorithms, *Physica D* 60 (1–4) (1992) 259–268. [doi:10.1016/](https://doi.org/10.1016/0167-2789(92)90242-F)
457 [0167-2789\(92\)90242-F](https://doi.org/10.1016/0167-2789(92)90242-F).
- 458 [33] V. Tsurkov, An analytical model of edge protection under noise suppres-
459 sion by anisotropic diffusion, *Journal of Computer and Systems Sciences*
460 *International* 39 (3) (2000) 437–440.
- 461 [34] S. Kichenassamy, The Perona-Malik method as an edge pruning algorithm,
462 *Journal of Mathematical Imaging and Vision* 30 (2) (2008) 209–219. [doi:](https://doi.org/10.1007/s10851-007-0029-2)
463 [10.1007/s10851-007-0029-2](https://doi.org/10.1007/s10851-007-0029-2).

- 464 [35] J. Kacur, K. Mikula, Slow and fast diffusion effects in image processing,
465 Computing and Visualization in Science 3 (4) (2001) 185–195. doi:10.
466 1007/s007910000047.
- 467 [36] V. B. S. Prasath, A well-posed multiscale regularization scheme for digital
468 image denoising, International Journal of Applied Mathematics and Com-
469 puter Science 21 (4) (2011) 769–777. doi:10.2478/v10006-011-0061-7.
- 470 [37] V. B. S. Prasath, A. Singh, An adaptive anisotropic diffusion scheme for
471 image restoration and selective smoothing, International Journal of Image
472 and Graphics 12 (1) (2012) 18pp. doi:10.1142/S0219467812500039.
- 473 [38] G. Gilboa, N. Sochen, Y. Y. Zeevi, Variational denoising of partly textured
474 images by spatially varying constraints, IEEE Transactions on Image Pro-
475 cessing 15 (8) (2006) 2281–2289. doi:10.1109/TIP.2006.875247.
- 476 [39] L. Alvarez, J. Esclarín, Image quantization using reaction-diffusion equa-
477 tions, SIAM Journal on Applied Mathematics 57 (1) (1997) 153–175.
478 doi:10.1137/S0036139994277580.
- 479 [40] M. G. Crandall, H. Ishii, P.-L. Lions, User’s guide to viscosity solu-
480 tions of second order partial differential equations, American Mathe-
481 matical Society Bulletin New Series 27 (1) (1992) 1–67. doi:10.1090/
482 S0273-0979-1992-00266-5.
- 483 [41] R. A. Horn, C. R. Johnson, Matrix analysis, Cambridge University Press,
484 Cambridge, UK, 1985.
- 485 [42] O. A. Ladyženskaja, V. A. Solonnikov, N. N. Ural’ceva, Linear and quasilin-
486 ear equations of parabolic type, Translated from the Russian by S. Smith.
487 Translations of Mathematical Monographs, Vol. 23, American Mathemat-
488 ical Society, Providence, R.I., USA, 1967.
- 489 [43] L. Alveraz, P. L. Lions, J.-M. Morel, Image selective smoothing and edge
490 detection by nonlinear diffusion II, SIAM Journal on Numerical Analysis
491 29 (3) (1992) 845–866. doi:10.1137/0729052.

- 492 [44] X. Li, T. Chen, Nonlinear diffusion with multiple edginess thresholds, Pat-
493 tern Recognition 27 (8) (1994) 1029–1037. doi:10.1016/0031-3203(94)
494 90142-2.
- 495 [45] F. Voci, S. Eiho, N. Sugimoto, H. Sekiguchi, Estimating the gradient
496 threshold in the Perona–Malik equation, IEEE Signal Processing Maga-
497 zine 21 (3) (2004) 39–46. doi:10.1109/MSP.2004.1296541.
- 498 [46] J. Weickert, Anisotropic diffusion in image Processing, B.G. Teubner-
499 Verlag, Stuttgart, Germany, 1998.
- 500 [47] J. Weickert, Coherence–enhancing diffusion filtering, International Jour-
501 nal of Computer Vision 31 (2–3) (1999) 111–127. doi:10.1023/A:
502 1008009714131.
- 503 [48] J. Kacur, K. Mikula, Slowed anisotropic diffusion, in: First International
504 Conference on Scale-Space Theory in Computer Vision, Vol. 1252, Utrecht,
505 The Netherlands, 1997, pp. 357–360, springer LNCS Eds.: Bart ter Haar
506 Romeny, Luc Florack, Jan Koenderink and Max Viergever. doi:10.1007/
507 3-540-63167-4_71.
- 508 [49] Z. Wang, A. C. Bovik, H. R. Sheikh, E. P. Simoncelli, Image quality assess-
509 ment: from error visibility to structural similarity, IEEE Transactions on
510 Image Processing 13 (4) (2004) 600–612. doi:10.1109/TIP.2003.819861.
511 URL <http://ece.uwaterloo.ca/~z70wang/research/ssim/>
- 512 [50] C. A. Z. Barcelos, M. Batista, Image restoration using digital inpainting
513 and noise removal, Image and Vision Computing 25 (1) (2007) 61–69. doi:
514 10.1016/j.imavis.2005.12.008.
- 515 [51] T. Barbu, V. Barbu, A PDE approach to image restoration problem with
516 observation on a meager domain, Nonlinear Analysis: Real World Appli-
517 cations 13 (3) (2012) 1206–1215. doi:10.1016/j.nonrwa.2011.09.014.